

# An acoustic streaming instability in thermoacoustic devices utilizing jet pumps

S. Backhaus<sup>a)</sup> and G. W. Swift

*Condensed Matter and Thermal Physics Group, Los Alamos National Laboratory, Los Alamos, New Mexico 87545*

(Received 30 August 2002; accepted for publication 29 November 2002)

Thermoacoustic-Stirling hybrid engines and feedback pulse tube refrigerators can utilize jet pumps to suppress streaming that would otherwise cause large heat leaks and reduced efficiency. It is desirable to use jet pumps to suppress streaming because they do not introduce moving parts such as bellows or membranes. In most cases, this form of streaming suppression works reliably. However, in some cases, the streaming suppression has been found to be unstable. Using a simple model of the acoustics in the regenerators and jet pumps of these devices, a stability criterion is derived that predicts when jet pumps can reliably suppress streaming. © 2003 Acoustical Society of America. [DOI: 10.1121/1.1543588]

PACS numbers: 43.25.Nm, 43.35.Ud [MFH]

## I. INTRODUCTION

Recently, thermoacoustic-Stirling hybrid engines<sup>1-4</sup> and refrigerators<sup>4,5</sup> that utilize traveling-wave phasing have been investigated. These devices are composed of a sandwich of three heat exchangers embedded in a looped acoustic network. The heat exchangers include an ambient heat exchanger, a stack or regenerator, and a heat exchanger at the “working” temperature which is above or below ambient depending on whether the device is an engine or refrigerator. These devices are filled with a thermodynamic working fluid, typically a pressurized ideal gas. The looped acoustic network may have distributed impedances, i.e., may have propagation lengths on the order of an acoustic wavelength,<sup>3</sup> or it may have lumped elements, i.e., with lengths much shorter than 1/4 of an acoustic wavelength.<sup>1,2,4,5</sup> In this article, the focus will be on engines and refrigerators that utilize regenerators embedded in a lumped-element acoustic network, because an engine of this type has already demonstrated high efficiency and refrigerators of this type promise higher efficiencies than existing orifice pulse tube refrigerators (OPTRs) at noncryogenic temperatures. A schematic drawing of a general lumped-element device is shown in Fig. 1. These devices are referred to as thermoacoustic-Stirling hybrid engines (TASHEs) and feedback pulse tube refrigerators (FPTRs).

Both TASHEs and FPTRs rely on their lumped acoustic networks for two roles. First, the network allows acoustic power to feed back from the working-temperature end of the regenerator to the ambient end. In an OPTR, this power is dissipated in an acoustic resistance at room temperature, while the acoustic network of an FPTR recycles this power into the ambient end of the regenerator.<sup>5</sup> This reduces the input power requirement and increases the efficiency of an FPTR compared to an OPTR.<sup>6</sup> In a TASHE, the acoustic power circulating in the acoustic network takes the place of mechanical components in various types of Stirling engines,

such as cranks, linkages, or pistons, reducing the mechanical complexity of the engine.<sup>2</sup> In both devices, the second role of the network is to set the magnitude and phase of the acoustic impedance in the regenerator. By shifting the phase of the velocity oscillation by  $\approx 90^\circ$ , the network transforms the standing-wave phasing in the resonator into nearly traveling-wave phasing in the regenerator. Also, the network keeps the magnitude of the acoustic impedance high so that viscous losses in the regenerator are reduced to an acceptable level.<sup>2,5</sup>

Although the lumped acoustic network makes both the TASHE and FPTR possible, it also introduces a complication. The network is essentially a wide-open tube that connects one end of the regenerator to the other. This topology allows for acoustic streaming, a steady flow of mass, around the looped network and through the regenerator. In fact, the acoustic power circulating around the looped network inherently encourages such streaming<sup>7</sup> in the direction from the ambient heat exchanger, through the regenerator, and to the working heat exchanger. A steady mass flow, no matter its direction, causes a heat leak to (FPTR) or from (TASHE) the working heat exchanger, drastically lowering the efficiency of both the TASHE and FPTR.

To combat this, a membrane or bellows could be used to block streaming around the loop while permitting oscillatory flow, but this might compromise the reliability inherent in a device that would otherwise have no moving parts. Alternatively, a nonlinear device termed a jet pump can be used to generate a time-averaged pressure, imposing low pressure at the ambient end of the regenerator so as to oppose the inherent tendency to stream. Typically, the geometry of the jet pump can be adjusted until the absence of streaming is indicated by a nearly linear temperature distribution through the regenerator.<sup>2,5</sup> In all TASHEs<sup>2,8-10</sup> that we have constructed to date, this technique has worked reliably. In contrast, one FPTR<sup>11</sup> that we have constructed demonstrated peculiar behavior. In that FPTR, it was impossible to adjust the geometry of the jet pump to stably cancel the streaming mass flux. By observing the temperature distribution in the regenerator, it was clear that there was always vigorous acoustic stream-

<sup>a)</sup>Electronic mail: backhaus@lanl.gov

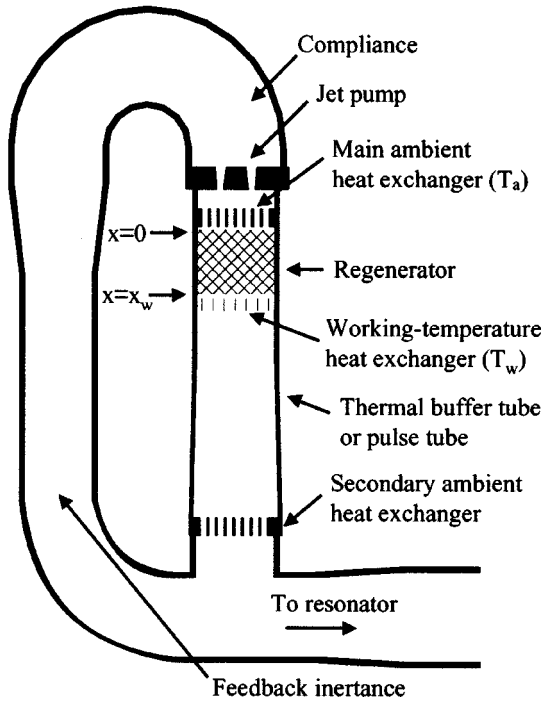


FIG. 1. Schematic drawing of a lumped-element FPTR or TASHE. An FPTR consumes acoustic power from the resonator and produces cooling at the working-temperature heat exchanger. Acoustic power that exits the working-temperature heat exchanger is recycled via the feedback loop to the main ambient heat exchanger. A TASHE supplies acoustic power to the resonator and circulates acoustic power around the feedback loop. As the power flows through the regenerator, it is amplified. Power in excess of that needed to maintain the power circulation in the feedback loop flows into the resonator to drive an acoustic load. Both the TASHE and FPTR are filled with a pressurized gas that serves as the thermodynamic working substance.

ing in one direction or the other. Also, the system demonstrated a hysteresis indicative of some type of instability. In another FPTR,<sup>5</sup> some operating points were stable while others were unstable.

The rest of this article presents a calculation that predicts when a TASHE or FPTR with a jet pump to suppress streaming is unstable to small perturbations. The few experimental observations described above are roughly consistent with these predictions. The temperature dependences of viscosity and density are key aspects of the calculation. If a small temperature change occurs in the heart of the regenerator, the viscosity and density will change and so the flow velocities through the regenerator may change. If the streaming mass flow changes in a direction that causes a temperature change in the heart of the regenerator of the same sign as the original change, positive feedback occurs and the streaming can grow catastrophically. The instabilities observed in some double-inlet pulse tube refrigerators<sup>12,13</sup> may also be due in part to this mechanism.

## II. STEADY-STATE SOLUTION

The instability is investigated using a typical linear perturbation approach, where the acoustic variables are taken to be their equilibrium values plus a small perturbation. Using the usual acoustic expansion and time-harmonic notation,<sup>14</sup> the steady-state solution can be written

$$p(x,t) = p_m + \text{Re} [p_1(x)e^{i\omega t}] + p_{2,0}(x), \quad (1)$$

$$U(x,t) = \text{Re} [U_1(x)e^{i\omega t}] + U_{2,0}(x), \quad (2)$$

$$T(x,t) = T_m(x) + \text{Re} [T_1(x)e^{i\omega t}], \quad (3)$$

where  $p$ ,  $U$ , and  $T$  are the gas pressure, volumetric flow rate, and laterally spatially averaged temperature, respectively, variables with the subscript 1 are complex, and  $\text{Re}[\dots]$  signifies the real part. The subscript 2,0 indicates a second-order time-independent quantity. The angular frequency of the oscillation is  $\omega$ ,  $t$  is time, and  $x$  is the coordinate along the axis of the regenerator, with  $x=0$  at the ambient face and  $x=x_w$  at the working-temperature face. If the perimeter of the regenerator is well insulated, the steady-state second-order energy flux,  $\dot{H}_2$ , is independent of both  $x$  and  $t$ .<sup>14</sup>

A simplified model of the acoustics in the regenerator, which we summarize here, has been used to obtain relationships between the various steady-state terms.<sup>2</sup> If the compliance, or void volume, of the regenerator is neglected, and the density oscillations are taken as isothermal, mass conservation and the temperature dependence of gas density require that the volumetric flow rate  $U_1$  be given by

$$U_1(x) = U_1(0) \frac{T_m(x)}{T_a}, \quad (4)$$

where  $T_a = T_m(0)$  is the mean temperature of the gas at the ambient end of the regenerator. Throughout the rest of this article, the subscripts “ $a$ ” and “ $w$ ” refer to a mean variable evaluated at the ambient and working-temperature faces of the regenerator, respectively. The volumetric flow rate into the ambient end,  $U_1(0)$ , is estimated<sup>2</sup> using a simplified model of the feedback network, yielding

$$U_1(0) = \frac{\omega^2 LC}{R_m} p_1(0), \quad (5)$$

where  $L$  and  $C$  are the inertia and compliance in the feedback loop, respectively. Typically,  $\omega L < R_m$ , and terms of order  $(\omega L/R_m)^2$  have been dropped to simplify the calculation. Here,  $R_m$  is the flow resistance of the regenerator referenced to  $U_1(0)$ , i.e.,

$$R_m = \frac{\Delta p_{1,\text{regen}}}{U_1(0)} = \frac{R_0}{x_w} \int_0^{x_w} \left( \frac{T_m(x)}{T_a} \right)^{1+b} dx, \quad (6)$$

where  $R_0$  is the flow resistance of the regenerator when its entire length  $x_w$  is at  $T_a$  and  $\Delta p_{1,\text{regen}}$  is the change in  $p_1$  across the regenerator.<sup>2</sup> The precise value of  $R_0$  is not important in this calculation. The “1” in the exponent  $(1+b)$  takes into account the  $T_m$  dependence of density and  $U_1$  expressed in Eq. (4), and the “ $b$ ” in the exponent takes into account the temperature-dependent viscosity of the gas in the regenerator, i.e.,  $\mu(T_m) = \mu(T_a)[T_m(x)/T_a]^b$ . The expression for  $R_m$  is valid in the low-Reynolds-number limit for screen beds, parallel plates, and other typical regenerator geometries.<sup>15</sup> In most cases,  $|\Delta p_{1,\text{regen}}| \ll |p_1|$ , and, therefore,  $p_1(x) \approx p_1$ . Without loss of generality,  $p_1$  can be taken to be real. Equations (4) and (5) show that  $U_1(x)$  is also real. Other symbols with subscript 1 will continue to represent complex variables.

The steady-state time-averaged second-order mass flux<sup>16</sup> is given by

$$\dot{M}_{2,0} = \text{Re}[\rho_1 \tilde{U}_1]/2 + \rho_m U_{2,0}, \quad (7)$$

where  $\rho_m$  is the mean density of gas in the regenerator,  $\rho_1$  is the first-order complex density oscillation amplitude, and the tilde denotes complex conjugation. Inside the regenerator, the pressure oscillations are nearly isothermal. Neglecting the small deviations from isothermal and using the fact that  $U_1$  is real, the first term in  $\dot{M}_{2,0}$  can be written<sup>7</sup>  $(\rho_m/p_m)p_1 U_1/2$ , so that  $\dot{M}_{2,0} = (\rho_m/p_m)p_1 U_1/2 + \rho_m U_{2,0}$ . The second term in  $\dot{M}_{2,0}$  depends on the second-order, steady volumetric flow rate  $U_{2,0}$ , which is driven by gradients in the second-order steady pressure  $p_{2,0}$  and by source terms that involve time averages of two first-order quantities.<sup>16,17</sup> Waxler has shown<sup>17,18</sup> that the latter source terms are negligible compared to the gradients in  $p_{2,0}$  in a parallel-plate regenerator, and we assume that this holds true for other regenerator-pore geometries. The second-order momentum equation is then identical to the first-order momentum equation with  $d/dt$ ,  $U_{2,0}$ , and  $p_{2,0}$  replacing  $i\omega$ ,  $U_1$ , and  $p_1$ , respectively.

In a TASHE or FPTR, there can be several sources of  $p_{2,0}$  including, but not limited to, pipe bends, diffusers, and “tees.”<sup>2,5</sup> However, in a well-designed device, the major source of  $p_{2,0}$  will be the jet pump used to control the streaming. In the steady state,  $\dot{M}_{2,0} = 0$  and  $p_1(x)$  is assumed to be equal to  $p_1(0)$ , requiring  $|U_{2,0}|$  to have the same spatial and  $T_m(x)$  dependence as  $|U_1|$ . Therefore, the same definition of  $R_m$  also applies to  $U_{2,0}$ , i.e.,  $R_m = \Delta p_{2,0}/U_{2,0}(0)$ . Using these two results,  $\dot{M}_{2,0}$  at the ambient end of the regenerator can be written

$$\dot{M}_{2,0}(0) = \frac{\rho_a}{2p_m} p_1 U_1(0) + \rho_a \frac{\Delta p_{2,0}}{R_m}. \quad (8)$$

Since  $\partial \dot{M}_{2,0}/\partial x = 0$ , this also gives the value of  $\dot{M}_{2,0}$  throughout the regenerator. Although  $\dot{M}_{2,0} = 0$ , Eq. (7) is required later when the steady-state solution is perturbed. If the jet pump is located near the ambient end of the regenerator, the time-average pressure drop across the regenerator,  $\Delta p_{2,0}$ , will be given by<sup>5</sup>

$$\Delta p_{2,0} = - \frac{\rho_a [U_1(0)]^2}{8A_{jp}^2} (K_{\text{out}} - K_{\text{in}}), \quad (9)$$

where  $A_{jp}$  is the area of the small opening in the jet pump, and  $K_{\text{in}}$  and  $K_{\text{out}}$  are the minor loss coefficients for the two directions of flow through the jet pump. If the jet pump were located near the working-temperature heat exchanger instead of the ambient end, an additional multiplicative factor of  $T_w/T_a$  would appear in Eq. (9). As will be seen later [see, e.g., Eq. (36) and the surrounding discussion], any multiplicative scale factor in  $\Delta p_{2,0}$  that is unaffected by the perturbation does not affect the final result of the calculation.

### III. PERTURBED SOLUTION

Next, an exponentially growing or decaying perturbation is added to the equilibrium solution reviewed in the previous section, so that the complete solution is of the form

$$p(x,t) = p_m + p_1 \cos \omega t + p_{2,0}(x) + \delta p_{2,0}(x) e^{\epsilon t}, \quad (10)$$

$$U(x,t) = U_1(x) \cos \omega t + U_{2,0}(x) + \{\delta U_1(x) \cos \omega t + \delta U_{2,0}(x)\} e^{\epsilon t}, \quad (11)$$

$$T(x,t) = T_m(x) + \text{Re}[T_1(x) e^{i\omega t}] + \{\delta T_m(x) + \text{Re}[\delta T_1(x) e^{i\omega t}]\} e^{\epsilon t}, \quad (12)$$

$$R(t) = R_m + \delta R e^{\epsilon t}, \quad (13)$$

$$\dot{H}(x,t) = \dot{H}_2 + \delta \dot{H}(x) e^{\epsilon t}. \quad (14)$$

The perturbation includes both oscillating and nonoscillating terms. The oscillating terms are assumed to have the same frequency as the corresponding terms in the equilibrium solution and an amplitude that changes slowly, but exponentially, in time compared to the acoustic period, i.e.,  $|\epsilon| \ll \omega$ . This two-time-scale approach allows the explicit separation of the slow change of the instability from the rapid acoustic oscillations. Nonoscillating terms also change exponentially in time with the same time constant as the amplitudes of the oscillating terms. Note that  $\delta U_1$  can be taken to be real for the same reasons that  $U_1$  is taken to be real.

We assume that  $T_a$  and  $T_w$  are fixed by good heat exchange with external fluids that have high heat capacity or latent heat or with high-heat-capacity heat exchangers. In either case, the thermal reservoirs in or near the heat exchangers are large enough to adjust to a varying heat load without a significant change in temperature. We also assume  $\delta p_1$  and  $\delta \omega$  are zero. For an FPTR, these last two conditions can be regarded as simple consequences of how the system is driven, e.g., by a linear motor at fixed frequency and whatever electric current is required to keep  $p_1$  fixed. For a TASHE,<sup>2</sup> one can similarly assume that the complex load impedance is deliberately varied to keep  $\omega$  and  $p_1$  fixed.

The calculation begins with the energy flux  $\dot{H}$  through the regenerator. In the steady state of a well-insulated regenerator,  $d\dot{H}_2/dx = 0$ , meaning there is no build up of energy inside the regenerator.<sup>14</sup> If a small, time-dependent perturbation is present, this condition is relaxed and the energy equation takes the form

$$\frac{\partial}{\partial t} [(1-\phi)\rho_s c_s T_s A + \phi \rho_m c_v T_m A] = - \frac{\partial \dot{H}}{\partial x}, \quad (15)$$

where  $\rho_s$ ,  $c_s$ ,  $\phi$ ,  $A$ , and  $T_s$  are the regenerator solid density, heat capacity, porosity, cross-sectional area, and temperature, respectively, and  $c_v$  is the isochoric heat capacity of the gas. Essentially, this equation states that if there is a spatial variation in the energy flux through the regenerator, energy is accumulated or depleted temporally, resulting in a temperature change of the working gas and regenerator solid at that location. On the acoustic time scale, the temperature of the solid and gas are not necessarily equal. (In fact, oscillations of the gas temperature give rise to the major source of  $\dot{H}_2$ .<sup>14</sup>) However, on the slow time scale of the perturbation growth, the excellent thermal contact between the regenerator solid and the gas will enforce  $\delta T_s \approx \delta T_m$ . Also, in a typical regenerator, the heat capacity of the solid is much higher than the gas,<sup>19</sup> i.e.,  $\phi \rho_m c_v / (1-\phi) \rho_s c_s \ll 1$ . Substituting the equilib-

rium solution plus perturbation into Eq. (15) and using the two approximations above yields, at linear order in the perturbation,

$$\epsilon(1-\phi)\rho_s c_s A \delta T_m = -\frac{d\delta H}{dx}. \quad (16)$$

A typical solution of Eq. (16) would proceed as follows.<sup>20</sup> The steady-state solution plus perturbation would be substituted into the other governing equations, such as the momentum and continuity equations, and a system of differential equations relating  $\delta H(x)$  and  $\delta T_m(x)$  would be obtained. Next, a set of eigenfunctions would be found that satisfies both Eq. (16) and any boundary conditions imposed at  $x=0$  and  $x_w$ . These eigenfunctions would then be substituted back into Eq. (16) to determine the growth rate  $\epsilon$  for each eigenfunction. Conditions under which one of the growth rates becomes positive would indicate an instability. Although this procedure would find all possible conditions for linear instability, carrying it out in this case would prove quite difficult. The resulting system of differential equations is not one with constant coefficients and is quite complicated. Finding a full set of eigenfunctions would be tedious, if not impossible, without numerical computation. Also, the difficulty of the calculation would obscure the physical effects that cause the instability.

To avoid this difficulty, a much simpler approach that yields analytical results is used, although it does not explore all possible instabilities. First, Eq. (16) is integrated from  $x=0$  to  $x=x_w$ , eliminating the need to know the detailed form of  $d\delta H/dx$ . Information about  $\delta H$  is only required at the ends of the regenerator. Next, the  $x$  dependence of the temperature perturbation is taken to be

$$\delta T_m = \sum_{n=1}^{n=\infty} \Theta_n \sin(n\pi x/x_w). \quad (17)$$

Implicit in Eq. (17) is our assumption that the heat exchangers at either end of the regenerator hold the faces at  $x=0$  and  $x=x_w$  at their steady-state values. It should be noted that the individual terms in Eq. (17) are not eigenfunctions of this problem, so there will be interaction between the various terms. However, this interaction will not be included in the following analysis, and only the  $n=1$  term will be carried through. (Both of these simplifications are reasonable in light of the observed temperature distribution in the FPTR that demonstrated a streaming instability: The deviation from a linear temperature distribution resembled half of a sine wave.<sup>11</sup>) Substituting Eq. (17) into Eq. (16), setting  $\Theta_1 = \Theta$ , and integrating from  $x=0$  to  $x=x_w$  yields

$$\frac{2x_w}{\pi} \rho_s c_s (1-\phi) A \epsilon \Theta - [\delta H(0) - \delta H(x_w)] = 0, \quad (18)$$

where any temperature dependence of  $\rho_s c_s$  has been ignored.

Typically, regenerators are made from piles of stainless-steel mesh. However, to estimate which terms of  $\delta H$  are important, the analytic expression for  $\dot{H}_2$  in a parallel-plate regenerator will be used. Except for axial conduction through the regenerator solid, the various terms are expected to have

the same order-of-magnitude values in a screen-based regenerator. The steady-state energy flux consists of four terms<sup>14</sup>

$$\begin{aligned} \dot{H}_2(x) &= \frac{p_1 U_1}{2} \text{Re} \left[ 1 - \frac{f_\kappa - \tilde{f}_v}{(1+\sigma)(1-\tilde{f}_v)} \right] \\ &+ \frac{\rho_m c_p U_1^2 \text{Im}(f_\kappa + \sigma \tilde{f}_v)}{2\phi A \omega (1-\sigma^2) |1-f_v|^2} \frac{dT_m}{dx} \\ &- [\phi A k + (1-\phi) A k_s] \frac{dT_m}{dx} + \dot{M}_{2,0} c_p T_m \\ &\equiv \dot{H}_b + \dot{H}_c + \dot{H}_k + \dot{H}_m, \end{aligned} \quad (19)$$

where each term has been given its own symbol for convenience, and the fact that  $U_1$  is real has been used to simplify the expression. In the assumed steady-state solution,  $\dot{M}_{2,0} = 0$ , and therefore  $\dot{H}_m = 0$ . However,  $\delta \dot{M}_{2,0}$  and its associated enthalpy flux,  $\delta \dot{H}_m$ , need not be zero. Since  $\delta T_m(0) = \delta T_m(x_w) = 0$ , the gas properties and  $f$  functions at  $x=0$  and  $x=x_w$  do not change, and  $\delta \dot{H}(0)$  can be written

$$\begin{aligned} \delta \dot{H}(0) &= \dot{H}_b(0) \frac{\delta U_1(0)}{U_1(0)} + \dot{H}_c(0) \left[ 2 \frac{\delta U_1(0)}{U_1(0)} \right. \\ &+ \left. \frac{1}{\nabla T_m|_{x=0}} \frac{d\delta T_m}{dx} \right]_0 + \frac{\dot{H}_k(0)}{\nabla T_m|_{x=0}} \frac{d\delta T_m}{dx} \Big|_0 \\ &+ \delta \dot{M}_{2,0}(0) c_p T_a \\ &\equiv \delta \dot{H}_b(0) + \delta \dot{H}_c(0) + \delta \dot{H}_k(0) + \delta \dot{H}_m(0), \end{aligned} \quad (20)$$

and similarly for  $\delta \dot{H}(x_w)$ .

As long as  $2\delta U_1(0)/U_1(0)$  and  $(d\delta T_m/dx)|_{x=0}/\nabla T_m|_{x=0}$  do not cancel or sum to a value much smaller than either individual term,  $\delta \dot{H}_b(0)$ ,  $\delta \dot{H}_c(0)$ , and  $\delta \dot{H}_k(0)$  can be compared simply by comparing the magnitudes of  $\dot{H}_b$ ,  $\dot{H}_c$ , and  $\dot{H}_k$ . For  $T_w < T_a$ , both terms have the same sign. However, for  $T_w > T_a$ , they have opposite signs. In this case, Eqs. (5), (17), (29), and (37) can be used to show that the sum of these two terms is never small compared to the either of individual terms themselves.

To compare  $\dot{H}_c$  and  $\dot{H}_k$ ,  $\dot{H}_c$  is expanded in the limit  $(r_h/\delta_\kappa)^2 \approx (r_h/\delta_v)^2 \ll 1$ , where  $\delta_\kappa$  and  $\delta_v$  are the thermal and viscous penetration depths and  $r_h$  is hydraulic radius.<sup>21</sup> This expansion is equally valid at low Reynolds numbers in screen-based regenerators where  $r_h$  is a rough measure of the average spacing between screen wires. In typical regenerators  $(r_h/\delta_\kappa)^2 \leq 0.1$ . After a small amount of algebra, the result is found to be

$$\dot{H}_c \approx -\frac{\rho_m c_p U_1^2}{2\phi A \omega} \left( \frac{r_h}{\delta_\kappa} \right)^2 \frac{dT_m}{dx}. \quad (21)$$

Taking the ratio of  $\dot{H}_k(0)$  with  $\dot{H}_c(0)$  yields

$$\frac{\dot{H}_k(0)}{\dot{H}_c(0)} \approx 2 \left( \frac{1-\phi}{\phi} \right) \left[ \frac{\delta_{\kappa,a}^2}{\xi_1(0) r_h} \right]^2 \frac{k_s}{k}, \quad (22)$$

where  $\xi_1(0)$  is the acoustic displacement amplitude and all terms are evaluated at the ambient end of the regenerator. Substituting typical numbers  $k_s/k \approx 100$ ,  $(\delta_\kappa/r_h)^2 \approx 10$ ,  $\delta_\kappa/\xi_1(0) \approx 0.01$ , and  $\phi \approx 0.7$  yields  $\dot{H}_k/\dot{H}_c \approx 0.1$ . In a screen-bed regenerator, this ratio is expected to be even smaller due to the poor thermal contact between screen layers.<sup>22</sup> Therefore,  $\delta\dot{H}_k(0) \ll \delta\dot{H}_c(0)$  and can be neglected in the right-hand side of Eq. (20).

To compare  $\delta\dot{H}_b(0)$  with  $\delta\dot{H}_c(0)$ ,  $\dot{H}_b$  is expanded in the limit  $(r_h/\delta_\kappa)^2 \rightarrow 0$ ,

$$\dot{H}_b \approx \left(\frac{r_h}{\delta_\kappa}\right)^4 \frac{p_1 U_1}{3}. \quad (23)$$

Taking the ratio of  $\dot{H}_b$  with  $\dot{H}_c$  at the ambient end of the regenerator yields

$$\left|\frac{\dot{H}_b(0)}{\dot{H}_c(0)}\right| \approx 4\phi(\gamma-1)\Gamma\left(\frac{r_h}{\delta_{\kappa,a}}\right)^2 \frac{x_w}{\lambda_a} \frac{T_a}{\Delta T_m}. \quad (24)$$

Here,  $\gamma$  is the ratio of specific heats,  $\lambda$  is the acoustic wavelength,  $\Delta T_m$  is the total temperature difference across the regenerator,  $\Gamma = (p_1/U_1)/(\rho_a c_a/A)$ , and  $\rho_a$  and  $c_a$  are the gas density and speed of sound at the ambient end. Substituting typical numbers  $\phi \approx 0.7$ ,  $\gamma-1 \approx 0.67$ ,  $(r_h/\delta_\kappa)^2 \approx 0.1$ ,  $x_w/\lambda \approx 0.005$ ,  $T_a/\Delta T_m \approx 1$ , and  $\Gamma \approx 10$  yields  $|\dot{H}_b(0)/\dot{H}_c(0)| \approx 0.01$ . Therefore,  $\delta\dot{H}_b(0) \ll \delta\dot{H}_c(0)$  and can be neglected in the right-hand side of Eq. (20).

Finally,  $\delta\dot{H}_c(0)$  is compared with  $\delta\dot{H}_m(0)$ . More specifically,  $\dot{H}_c(0)\delta U_1(0)/U_1(0)$  is compared with  $\delta\dot{M}_{2,0}(0)c_p T_a$ . To estimate  $\delta\dot{M}_{2,0}(0)$ , only one component is used, namely  $\text{Re}[\rho_1(0)\delta\tilde{U}_1(0)]/2$ . Assuming an isothermal density oscillation, the ratio of the two terms is

$$\frac{\delta\dot{M}_{2,0}(0)c_p T_a}{\dot{H}_c(0)\delta U_1(0)/U_1(0)} \approx 10 \frac{\gamma\phi}{\sigma} \frac{x_w}{\lambda} \left(\frac{\delta_\nu}{r_h}\right)^2 \frac{T_a}{\Delta T_m} \Gamma \approx 10, \quad (25)$$

where the numerical value results from substituting typical numbers given previously. The approximation  $\delta\dot{M}_{2,0}(0) \approx \text{Re}[\rho_1(0)\delta\tilde{U}_1(0)]/2$  most likely overestimates  $\delta\dot{M}_{2,0}(0)$ .

Now that  $\delta\dot{H}_c$  and  $\delta\dot{H}_m$  have been established as the dominant terms in  $\delta\dot{H}$ , it remains to calculate these terms at either end of the regenerator. At  $x=0$  and  $x=x_w$ ,  $\delta\dot{H}_c$  is given by

$$\delta\dot{H}_c(0) = \dot{H}_c(0) \left[ 2 \frac{\delta U_1(0)}{U_1(0)} + \frac{1}{\nabla T_m|_0} \frac{d\delta T_m}{dx} \Big|_0 \right], \quad (26)$$

$$\delta\dot{H}_c(x_w) = \dot{H}_c(x_w) \left[ 2 \frac{\delta U_1(x_w)}{U_1(x_w)} + \frac{1}{\nabla T_m|x_w} \frac{d\delta T_m}{dx} \Big|_{x_w} \right]. \quad (27)$$

In the steady state,  $\dot{H}_c \gg \dot{H}_b$ ,  $\dot{H}_c \gg \dot{H}_k$  and  $\dot{H}_m = 0$ . Therefore,  $\dot{H}_c(0) \approx \dot{H}_c(x_w) \equiv \dot{H}_c$ . Also,  $\delta U_1(0)/U_1(0) = \delta U_1(x_w)/U_1(x_w)$ . The difference in  $\delta\dot{H}_c$  across the regenerator, needed for Eq. (18), is then

$$\delta\dot{H}_c(0) - \delta\dot{H}_c(x_w)$$

$$= \dot{H}_c \left[ \frac{1}{\nabla T_m|_0} \frac{d\delta T_m}{dx} \Big|_0 - \frac{1}{\nabla T_m|x_w} \frac{d\delta T_m}{dx} \Big|_{x_w} \right]. \quad (28)$$

To be consistent with  $\dot{H}_c(0) = \dot{H}_c(x_w)$ , Eq. (21) shows that the mean temperature gradients at the two ends are related by

$$\nabla T_m|x_w = \tau^b \nabla T_m|_0, \quad (29)$$

where  $\tau = T_w/T_a$ . Using this in Eq. (28), the difference in  $\delta\dot{H}_c$  is found to be

$$\delta\dot{H}_c(0) - \delta\dot{H}_c(x_w) = \frac{\dot{H}_c}{\nabla T_m|_0} \frac{\pi}{x_w} (1 + \tau^{-b}) \Theta. \quad (30)$$

For both an FPTR and a TASHE, the term  $\dot{H}_c/\nabla T_m|_0$  is negative. Therefore, if the perturbation of the regenerator temperature is positive ( $\Theta > 0$ ), the effect of  $\delta\dot{H}_c$  is to remove energy and cool the regenerator. This effect, present in any Stirling-type engine or refrigerator whether or not a toroidal topology allows streaming, attempts to reduce any perturbation from the steady state, suppressing a possible instability.

Next, the effect of  $\delta\dot{H}_m$  is determined. The difference in  $\delta\dot{H}_m$  at the two regenerator faces is given by

$$\delta\dot{H}_m(0) - \delta\dot{H}_m(x_w) = \delta\dot{M}_{2,0}(0)c_p T_a - \delta\dot{M}_{2,0}(x_w)c_p T_w. \quad (31)$$

To proceed further, a relationship between  $\delta\dot{M}_{2,0}(0)$  and  $\delta\dot{M}_{2,0}(x_w)$  must be determined. In the steady-state solution, the time-averaged continuity equation<sup>16</sup> reveals that since  $\delta\rho_m/\delta t = 0$ ,  $\dot{M}_{2,0}(0) = \dot{M}_{2,0}(x_w)$ . For  $\delta\dot{M}_{2,0}$ , it is not clear if this relationship still holds. Let  $\alpha = \delta\dot{M}_{2,0}(0) - \delta\dot{M}_{2,0}(x_w)$ . If  $\alpha \neq 0$ , then the density of the gas in the regenerator must be changing, i.e.,  $\alpha \approx \phi A x_w \epsilon \delta\rho_m$ . This change in density is driven by either a change in mean temperature or a change in mean pressure. Considering a change in mean temperature,

$$\alpha \approx \phi A x_w \rho_m \frac{\epsilon \delta T_m}{T_m}. \quad (32)$$

However, for  $\delta T_m$  to change in the first place, there must be a  $\delta\dot{M}_{2,0}$  given by

$$(1 - \phi)\rho_s c_s A x_w \epsilon \delta T_m \approx \delta\dot{M}_{2,0} c_p (T_w - T_a). \quad (33)$$

Combining the last two equations yields

$$\frac{\alpha}{\delta\dot{M}_{2,0}} \approx \frac{\phi \rho_m c_p}{(1 - \phi)\rho_s c_s} \frac{T_w - T_a}{T_m} \ll 1, \quad (34)$$

showing that, to a good approximation,  $\delta\dot{M}_{2,0}(0) = \delta\dot{M}_{2,0}(x_w)$ . Therefore, the difference in  $\delta\dot{H}_m$  at the two ends of the regenerator can be written

$$\delta\dot{H}_m(0) - \delta\dot{H}_m(x_w) = \delta\dot{M}_{2,0}(0)c_p T_a (1 - \tau). \quad (35)$$

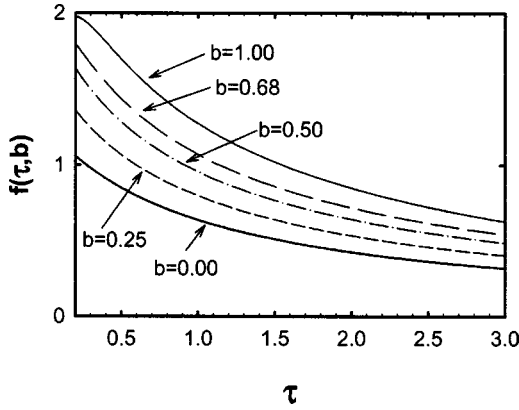


FIG. 2. A plot of  $f(\tau, b)$  for various values of  $b$ . For helium,  $b \approx 0.68$ . The integrals in Eq. (37) are performed numerically.

Perturbing Eq. (7) and using  $\dot{M}_{2,0} = 0$  in the steady state,  $\delta U_1(0)/U_1(0) = -\delta R/R_m$  from Eq. (5), and  $\delta \Delta p_{2,0}/\Delta p_{2,0} = -2\delta R/R_m$  from Eq. (9) yields

$$\delta \dot{M}_{2,0}(0) = -\frac{\rho_a}{p_m} \frac{p_1 U_1(0)}{2} \frac{\delta \Delta p_{2,0}}{\Delta p_{2,0}} = \frac{2\rho_a}{p_m} \dot{E}_2(0) \frac{\delta R}{R_m}, \quad (36)$$

where  $\dot{E}_2(0)$  is the acoustic power flowing into the ambient end of the regenerator.  $\delta R/R_m$  is calculated by perturbing Eq. (6):

$$\frac{\delta R}{R_m} = \frac{(1+b) \int_0^{x_w} T_m^b(x) \sin(\pi x/x_w) dx}{\int_0^{x_w} T_m^{1+b}(x) dx} \Theta = \frac{\Theta}{T_a} f(\tau, b), \quad (37)$$

where, to be consistent with Eq. (29),  $T_m(x)$  is approximated by

$$T_m(x) = T_a \left[ 1 + (\tau - 1) \frac{x}{x_w} - \frac{\tau - 1}{\pi} \frac{\tau^b - 1}{\tau^b + 1} \sin\left(\frac{\pi x}{x_w}\right) \right], \quad (38)$$

and the variable of integration is changed to  $d(x/x_w)$ . A plot of  $f(\tau, b)$  for various values of  $b$  is shown in Fig. 2. Finally, combining Eqs. (35), (36), and (37) yields

$$\delta \dot{H}_m(0) - \delta \dot{H}_m(x_w) = \frac{2\gamma}{\gamma - 1} (1 - \tau) f(\tau, b) \dot{E}_2(0) \frac{\Theta}{T_a}. \quad (39)$$

From Eq. (39) it is clear what drives the instability. For  $\Theta > 0$ , the sign of the right-hand side of this expression is determined by  $(1 - \tau)$ . All other factors are positive. For a TASHE,  $(1 - \tau)$  is negative and the perturbed time-average mass flux removes energy from the regenerator, reducing the original perturbation. For an FPTR,  $(1 - \tau)$  is positive and energy is dumped into the regenerator, amplifying the perturbation. Equation (30) already showed that no matter the value of  $\tau$ ,  $\delta \dot{H}_c$  reduces the original perturbation. For  $\tau > 1$ , i.e., a TASHE, a jet pump can reliably be used to suppress streaming. For  $\tau < 1$ , i.e., an FPTR, there exists a possibility of an instability with  $\delta \dot{H}_c$  competing with  $\delta \dot{H}_m$ .

Now that the term that drives the instability is identified, the cause can be investigated. In either an FPTR or a

TASHE, if  $\Theta$  is positive, the average temperature of the regenerator increases slightly and its resistance grows, reducing  $U_1(0)$ . The effect on the two terms in Eq. (7) is slightly different. The smaller  $U_1(0)$  results in a lower  $\text{Re}[\rho_1(0)\tilde{U}_1(0)]/2$ , but  $|U_{2,0}|$  decreases even more because it varies as  $U_1^2(0)$  through its dependence on  $\Delta p_{2,0}$ . Therefore, when the regenerator warms slightly,  $\dot{M}_{2,0}$  increases slightly, i.e.,  $\delta \dot{M}_{2,0}(0) > 0$ . In a TASHE, this blows ambient gas into the regenerator, cooling it down and suppressing any instability. In an FPTR, the ambient gas warms the regenerator further, creating an instability.

Combining Eqs. (18), (30), and (39) gives an equation for the growth rate of the perturbation

$$\frac{2}{\pi} \rho_s c_s T_a (1 - \phi) A x_w \epsilon = \frac{\pi(T_a/x_w)}{\nabla T_m|_0} (1 + \tau^{-b}) \dot{H}_c + \frac{2\gamma}{\gamma - 1} (1 - \tau) f(\tau, b) \dot{E}_2(0). \quad (40)$$

If the right-hand side of this equation is positive, the perturbation will grow exponentially and an instability results with a large streaming mass flux around the lumped-element loop. If it is negative, the perturbation decays and the jet pump controls the streaming in a stable manner. As already discussed, both terms on the right-hand side are negative for a TASHE. Therefore, a jet pump can be used in a TASHE with confidence that it will always control the streaming. In an FPTR, the first term is negative and the second is positive. Therefore, they must be compared to see when an instability results.

To make this comparison more transparent,  $\dot{E}_2(0)$  is expressed in terms of the gross cooling power of the FPTR, i.e.,  $\dot{Q}_{c,\text{gross}} \approx \tau \dot{E}_2(0)$ .<sup>6</sup> The right-hand side of Eq. (40) is positive when

$$\frac{\dot{H}_c}{\dot{Q}_{c,\text{gross}}} < \frac{2}{\pi} \frac{\gamma}{\gamma - 1} \frac{(\tau - 1) f(\tau, b)}{(1 + \tau^{-b}) \tau} \frac{\nabla T_m|_0}{(T_a/x_w)}. \quad (41)$$

Because  $\nabla T_m|_{x_w} = \tau^b \nabla T_m|_0$ , the term  $\nabla T_m|_0/(T_a/x_w)$  is given by  $2(\tau - 1)/(1 + \tau^b)$ . Substituting this result into Eq. (41), the final result is

$$\frac{\dot{H}_c}{\dot{Q}_{c,\text{gross}}} < \frac{4}{\pi} \frac{\gamma}{\gamma - 1} \frac{(\tau - 1)^2 f(\tau, b)}{(1 + \tau^b)(1 + \tau^{-b}) \tau}. \quad (42)$$

The right-hand side of Eq. (42) is computed as a function of  $\tau$  for  $\gamma = 5/3$  and  $b = 0$ ,  $b = 0.68$  (typical for helium), and  $b = 0.85$  (typical for argon). The results are shown in Fig. 3. For FPTRs operating below and to the left of the lines, a jet pump *cannot* be used to control streaming in stable fashion. For FPTRs operating above and to the right of the lines, a jet pump will suppress streaming in a stable fashion. The open squares in Fig. 3 are two different operating points from a  $\approx 2$ -kW FPTR intended to liquefy natural gas.<sup>11</sup> The jet pump in this FPTR never was able to reliably control the streaming. Since this FPTR used helium as its working gas, the squares should be compared to the  $b = 0.68$  line. The circles are from an earlier benchtop FPTR.<sup>5</sup> The filled circles

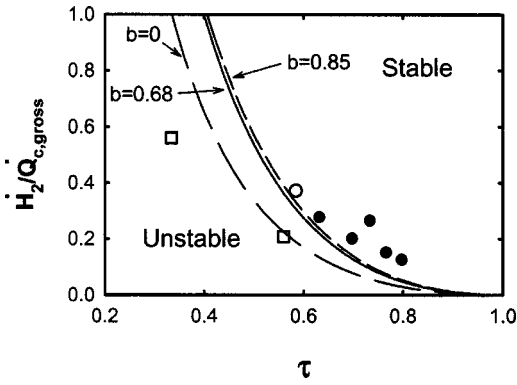


FIG. 3. Stability curve. The lines are the threshold of instability when the left-hand side of Eq. (42) equals the right-hand side for  $b=0$ ,  $b=0.68$ , and  $b=0.85$ . As shown by Eqs. (22) and (24),  $\dot{H}_k$  and  $\dot{H}_b$  are much smaller than  $\dot{H}_c$  so that  $\dot{H}_2 \approx \dot{H}_c$ . Below and left of these lines, a jet pump will not suppress streaming in a stable manner. The open squares left of the line are data from an FPTR that demonstrated a streaming instability (Ref. 11) and should be compared with the  $b=0.68$  line. The circles are from an earlier benchtop FPTR (Ref. 5). The filled circles are operating points where the jet pump controlled the streaming stably. The open circle is an operating point where the streaming control was unstable. The circles should be compared to the  $b=0.85$  line. In both cases,  $\dot{H}_2$  and  $\dot{Q}_{c, \text{gross}}$  are not directly measured. They are calculated using DeltaE (Ref. 24).

are operating points where the streaming control was stable. The open circle is an operating point with unstable streaming control. This FPTR used argon as a working gas, so the circles should be compared with the  $b=0.85$  line.

To be consistent with the steady-state condition  $\dot{H}_c(0) = \dot{H}_c(x_w)$  and the neglect of regenerator compliance in Eq. (5), the approximate mean temperature given in Eq. (38) was used throughout the calculation. However, in actual hardware where the compliance of the regenerator may be important or the phase of  $U_1(0)$  relative to  $p_1$  may be significantly different from zero,  $T_m(x)$  may deviate from the temperature profile used in the calculation. The calculation has been redone for a linear temperature profile, i.e., a constant  $\nabla T_m(x)$ . There are differences with the results shown in Fig. 3, but they are small enough not to be noticeable on the plot. The result that a TASHE is always stable still holds for a linear temperature profile as well.

#### IV. CONCLUSION

Using a simplified model of the acoustics in the regenerator of a TASHE and FPTR, the stability of jet pump control of streaming has been investigated. A stability criterion has been derived and found to be in agreement with the meager data available to date. The stability criterion shows that jet pump control of streaming is stable for all TASHEs. It also provides a threshold temperature ratio below which streaming control in a FPTR is unstable. The mathematics is based on analyzing how the temperature in the center of the regenerator responds to changes in streaming flows through the regenerator, which are themselves controlled by the temperature in the center of the regenerator. The analysis shows that two effects dominate.

First, ordinary second-order energy flow through the regenerator, whose largest term is proportional to  $U_1^2 dT_m/dx$ ,

always exerts a stabilizing influence. If the temperature of the center of the regenerator of a TASHE decreases a small amount, enthalpy flow from the hot end to the center increases as the average temperature gradient in the hot half steepens, and enthalpy flow from the center to the ambient end decreases as the average temperature in the cooler half becomes more shallow; both of these changes in enthalpy flow tend to raise the temperature in the center, canceling the original, assumed decrease in temperature. Similar arguments for an assumed small increase in the center temperature, and for an FPTR instead of a TASHE, also lead to cancellation, and, hence, stability.

Second, the temperature dependences of the viscosity and density of the gas in the regenerator cause a change in streaming that affects that very temperature. In an FPTR, this effect is destabilizing. If the temperature of the center of the regenerator of an FPTR decreases a small amount, the viscosity decreases and the density increases; both of these changes reduce  $R$ , leading to increases in both  $U_1$  and  $U_{2,0}$ . If  $\Delta p_{2,0}$  exerted by the jet pump were to remain constant, the fractional changes in  $U_1$  and  $U_{2,0}$  would be equal to the fractional change in  $R$ , and the streaming—a balance between  $U_1$  and  $U_{2,0}$ —would change little. However,  $\Delta p_{2,0}$  does not remain constant; it increases, thereby changing the streaming in a direction that carries cold gas into the regenerator, amplifying the original temperature decrease. A similar argument for a TASHE leads instead to stability.

Operation of a cryogenic FPTR with deliberately large  $\dot{H}_2$  to enforce stability is very undesirable, because nonzero  $\dot{H}_2$  consumes cooling power, reducing efficiency. However, the present analysis hints at ways that the stability curve might be shifted slightly. Three examples will be mentioned. First, the analysis assumed that  $K_{\text{out}}$ ,  $K_{\text{in}}$ , and  $A_{jp}$  in Eq. (9) are independent of amplitude. If one or more of these coefficients depended on  $U_1$ , either via hydrodynamics or elastic motion of the jet pump walls, a region of enhanced stability could be created. Second, Eq. (42) shows that reduced  $\gamma$  or increased  $b$  improves stability. Third, the analysis assumed that  $R$ ,  $f_\kappa$ , and  $f_\nu$  are independent of velocity, but the more complicated, velocity-dependent flow resistance and heat transfer coefficient in screen beds may provide an opportunity for improved stability.

#### ACKNOWLEDGMENTS

This work was supported by the OBES/DMS in the U. S. Department of Energy's Office of Science.

- <sup>1</sup>S. Backhaus and G. W. Swift, "A thermoacoustic-Stirling heat engine," *Nature (London)* **399**, 335–338 (1999).
- <sup>2</sup>S. Backhaus and G. W. Swift, "A thermoacoustic-Stirling heat engine: Detailed study," *J. Acoust. Soc. Am.* **107**, 3148–3166 (2000).
- <sup>3</sup>T. Yazaki, A. Iwata, T. Maekawa, and A. Tominaga, "Traveling wave thermoacoustic engine in a looped tube," *Phys. Rev. Lett.* **81**, 3128–3131 (1998).
- <sup>4</sup>C. M. de Blok and N. A. H. J. van Rijt, Thermo-acoustic system, U. S. Patent No. 6,314,740, 13 Nov. 2001.
- <sup>5</sup>G. W. Swift, D. L. Gardner, and S. Backhaus, "Acoustic recovery of lost power in pulse tube refrigerators," *J. Acoust. Soc. Am.* **105**, 711–724 (1999).
- <sup>6</sup>P. Kittel, "Ideal orifice pulse tube refrigerator performance," *Cryogenics* **32**, 843–844 (1992).

- <sup>7</sup>D. Gedeon, “dc gas flows in Stirling and pulse-tube cryocoolers,” in *Cryocoolers 9*, edited by R. G. Ross (Plenum, New York, 1997), pp. 385–392.
- <sup>8</sup>S. Backhaus and G. W. Swift, “Fabrication and use of parallel plate regenerators in thermoacoustic engines,” in *Proceedings of the 36th Inter-society Energy Conversion Engineering Conference* (American Society of Mechanical Engineers, New York, 2001), pp. 453–458.
- <sup>9</sup>S. Backhaus, E. Tward, and M. Petach, “Thermoacoustic power systems for space applications,” in *Proceedings of the Space Technology and Applications International Forum 2002*, edited by M. El-Genk (Springer, New York, 2002), pp. 939–944.
- <sup>10</sup>Unpublished data from 2000 collaboration between Chart, Inc. and Los Alamos National Laboratory.
- <sup>11</sup>Unpublished data from 1999 collaboration between Chart, Inc. and Los Alamos National Laboratory.
- <sup>12</sup>J. R. Olson, V. Kotsubo, P. J. Champagne, and T. C. Nast, “Performance of a Two-State Pulse Tube Cryocooler for Space Applications,” in *Cryocoolers 10*, edited by R. G. Ross (Plenum, New York, 1999), pp. 163–170.
- <sup>13</sup>V. Kotsubo, P. Huang, and T. C. Nast, “Observation of dc flows in a double inlet pulse tube,” in *Cryocoolers 10*, edited by R. G. Ross (Plenum, New York, 1999), pp. 299–305.
- <sup>14</sup>G. W. Swift, *Thermoacoustics: A Unifying Perspective for some Engines and Refrigerators* (Acoustical Society of America, NY, 2002).
- <sup>15</sup>In regenerators, typical Reynolds numbers are on the order of 10 to 100. For parallel plates and circular or rectangular pores, the low-Reynolds number limit applies up to Reynolds numbers of  $\approx 1000$  or higher (Ref. 23) where a relatively sharp transition from laminar to turbulent flow is observed. However, the transition is not so sharp in screen beds. In this case, the flow can be characterized by a “laminar” flow resistance, i.e., one that does not depend on Reynolds number, and a turbulent flow resistance that increases linearly with Reynolds number (Ref. 19). For screen bed porosities in the range 0.65 to 0.75, the laminar and turbulent contributions are equal for Reynolds numbers of 90 to 130. This is the upper range of Reynolds numbers in regenerators. The data presented in this article are taken at Reynolds numbers of  $\approx 20$  (Ref. 5) and  $\approx 45$  (Ref. 11).
- <sup>16</sup>W. L. M. Nyborg, “Acoustic streaming,” in *Physical Acoustics*, edited by W. P. Mason (Academic, New York, 1965), Vol. IIB, p. 265.
- <sup>17</sup>R. Waxler, “Stationary velocity and pressure gradients in a thermoacoustic stack,” *J. Acoust. Soc. Am.* **109**, 2739–2750 (2001).
- <sup>18</sup>Waxler (Ref. 17) shows that  $dp_{2,0}/dx$  dominates other contributions to  $U_{2,0}$  by a factor of order  $(\delta_\kappa/r_h)^2$ , where  $\delta_\kappa$  is the thermal penetration depth and  $2r_h$  is the gap in the parallel-plate regenerator. This factor is always large for regenerators that are at least reasonably effective. The neglect of the temperature dependence of viscosity is not always acceptable in streaming calculations [see, e.g., J. R. Olson and G. W. Swift, “Acoustic streaming in pulse tube refrigerators: Tapered pulse tubes,” *Cryogenics* **37**, 769–776 (1997)]. Incorporating this effect into Waxler’s analysis adds a term  $\langle (\partial/\partial y)\mu_1\partial v_{1,x}/\partial y \rangle$  to his Eq. (21), in his notation. This term also turns out to be only of order  $(r_h/\delta_\kappa)^2$ .
- <sup>19</sup>G. W. Swift and W. C. Ward, “Simple harmonic analysis of regenerators,” *J. Thermophys. Heat Transfer* **10**, 652–662 (1996).
- <sup>20</sup>S. Chandrasekhar, *Hydrodynamic and Hydromagnetic Stability* (Dover, New York, 1961).
- <sup>21</sup>The hydraulic radius is the ratio of the gas volume to the gas–solid contact area. For example, for parallel plates  $r_h$  is half of the distance between the plates.
- <sup>22</sup>M. A. Lewis, T. Kuriyama, F. Kuriyama, and R. Radebaugh, “Measurement of heat conduction through stacked screens,” *Adv. Cryog. Eng.* **43**, 1611–1618 (1998).
- <sup>23</sup>W. M. Kays and A. L. London, *Compact Heat Exchangers* (McGraw-Hill, New York, 1964).
- <sup>24</sup>W. C. Ward and G. W. Swift, “Design environment for low amplitude thermoacoustic engines (DeltaE),” *J. Acoust. Soc. Am.* **95**, 3671–3672 (1994). Software and user’s guide available either from the Los Alamos thermoacoustics website at [www.lanl.gov/thermoacoustics/](http://www.lanl.gov/thermoacoustics/) or from the Energy Science and Technology Software Center, US Department of Energy, Oak Ridge, Tennessee.